Vibrational properties of epitaxial Bi_4Te_3 films as studied by Raman spectroscopy

Hao Xu,[1,2] Yuxin Song,[1,a] Wenwu Pan,[1,2] Qimiao Chen,[1,2] Xiaoyan Wu,[1,2] Pengfei Lu,[3] Qian Gong,[1] and Shumin Wang[1,4,a]
[1]*State Key Laboratory of Functional Materials for Informatics, Shanghai Institute of Microsystem and Information Technology, Chinese Academy of Sciences, 865 Changning Road, Shanghai 200050, China*
[2]*University of Chinese Academy of Sciences, No.19A Yuquan Road, Beijing 100049, China*
[3]*State Key Laboratory of Information Photonics and Optical Communications, Ministry of Education, Beijing University of Posts and Telecommunications, P.O. Box 72, Beijing 100876, China*
[4]*Department of Microtechnology and Nanoscience, Chalmers University of Technology, 41296 Gothenburg, Sweden*

(Received 24 April 2015; accepted 27 July 2015; published online 4 August 2015)

Bi_4Te_3, as one of the phases of the binary Bi–Te system, shares many similarities with Bi_2Te_3, which is known as a topological insulator and thermoelectric material. We report the micro-Raman spectroscopy study of 50 nm Bi_4Te_3 films on Si substrates prepared by molecular beam epitaxy. Raman spectra of Bi_4Te_3 films completely resolve the six predicted Raman-active phonon modes for the first time. Structural features and Raman tensors of Bi_4Te_3 films are introduced. According to the wavenumbers and assignments of the six eigenpeaks in the Raman spectra of Bi_4Te_3 films, it is found that the Raman-active phonon oscillations in Bi_4Te_3 films exhibit the vibrational properties of those in both Bi and Bi_2Te_3 films. [http://dx.doi.org/10.1063/1.4928217]

I. INTRODUCTION

Bi_2Te_3 has been predicted and experimentally confirmed to be a typical three-dimensional (3D) topological insulator (TI) material, and is expected to possess robust conducting surface states and an insulating gap in the bulk.[1,2] The unique surface states originating from strong spin-orbit coupling are topologically protected against backscattering by time reversal symmetry.[3] Bi_2Te_3 can thus potentially be used for quantum computing, magnetic memory and so forth.[4] Bi_2Te_3 is also known as a significant thermoelectric (TE) material owing to the highest figure-of-merit among all bulk materials at room temperature: $ZT = 1$.[5] This value can be further increased in low dimensional heterostructures[6] or through the thermoelectric superlattices.[7]

Numerous efforts[1–6] have been devoted to the study of Bi_2Te_3 as one phase of the binary Bi–Te system, which has often overshadowed the fact that the Bi–Te system exhibits various different phases, such as BiTe and Bi_4Te_3. It has been reported that there exists no less than seven phases of Bi_xTe_y in a compositional range between 40 and 75 .% Bi.[8] By contrast, all phases have a rhombohedral- or trigonal-layered structure at ambient conditions with very similar a-axis parameters (approximately 4.4 Å) while c-axis parameters vary from 10 Å to above 100 Å.[9] Bi_4Te_3, also known as pilsenite, is another representative phase of the binary Bi–Te system. Given the periodical crystal structure, Bi_4Te_3 can be written as $(Bi_2)_3(Bi_2Te_3)_3$.[10] Among the widely studied and superior thermoelectric materials are the long known Bi_2Te_3 and Bi based alloys, thus, it is essential to investigate the $(Bi_2)_m(Bi_2Te_3)_n$ homologous series. Additionally, a heterostructure formed by a Bi bilayer above Bi_2Te_3 has been shown to exhibit new TI phenomena,[11] thus, it is reasonable to expect

[a]E-mail address: songyuxin@mail.sim.ac.cn; shumin@chalmers.se

Bi_4Te_3, whose crystal structure contains almost the same Bi_2Te_3/Bi_2 heterostructure, to also be a TI with unique properties. We have found that different flux ratios of Te/Bi can lead to the phases of bismuth telluride between Bi_2Te_3 and Bi_4Te_3 when grown by molecular beam epitaxy (MBE).[12] The structural and electronic properties of these two phases are significantly different.[12] Other properties, for example, phonon scattering and phonon-electron interactions, are of great interest for both TI and TE applications.

Raman spectroscopy can provide useful information about inherent phonon oscillations, phonon-electron interactions and structural features down to the nanoscale, which will aid in the research on Bi_4Te_3. Despite the promising TI and TE properties of Bi_4Te_3, there has only been one report of the Raman spectra of Bi_4Te_3. Russo *et al.* reported the Raman spectra of Bi_4Te_3 polycrystalline thin films prepared by pulsed laser deposition, where only one peak was found.[13] In this work, we undertook Raman spectroscopy measurements from 50-nm-thick Bi_4Te_3 and Bi_2Te_3 films both grown on Si substrates by MBE. In the spectra of the Bi_4Te_3 films, all the six expected Raman-active phonon modes are observed and are resolved completely for the first time. Phonon oscillations involved in the Raman scattering in Bi_4Te_3 films are found to display the vibrational properties of those in both Bi and Bi_2Te_3 films.

II. EXPERIMENTAL DETAILS

The Bi_4Te_3 and Bi_2Te_3 thin films were grown on Si (111) substrates by MBE and details of the substrate preparation and growth can be found in Ref. 12. Both materials grew along their c-axis confirmed by X-ray diffraction (XRD), meaning that the quintuple layers (QLs) and the bilayer-Bi (Bi_2), which will be described in the next section, are parallel the substrate surface. Raman scattering experiments were conducted at room temperature, using a Horiba HR confocal micro-Raman spectrometer in the backscattering configuration excited with a Nd:YAG 532 nm laser, whose light spot diameter was around 1 μm. The resolution was approximately 1 cm^{-1} using the 1800 groove/mm grating. Since Bi_4Te_3 and Bi_2Te_3 have a low thermal conductivity and a low melting point, it is essential to control the laser power and irradiation time to avoid local heating effects (LHE) and melting-induced oxidation during the measurements. After many trials, the optimum excitation power of 2 mW (the irradiation laser power on the sample surface was much less than 2 mW) together with a 0.1 μm wide slit and exposure time of 100 s were found to provide the best signal-to-noise (S/N) ratio and effectively avoid heating-induced effects.

III. RESULTS AND DISCUSSION

A. Crystal structure and Raman tensors

Bi_4Te_3 has a rhombohedral crystal structure,[14] which is composed of double atomic layers of bismuth -Bi-Bi- lying between the QL -Te-Bi-Te-Bi-Te- slabs, as shown in Fig. 1(a). It can be seen that there exist two different Bi atoms with two different symmetry centers. The unit cell contains three Bi_2 slabs and three QL slabs, one third of which is arranged in the following order: - (Te^1-Bi^1-Te^2-Bi^1-Te^1)-(Bi^2-Bi^2)-. Atoms inside both the Bi_2 slabs and the QL slabs are covalently connected[15,16] whereas the interactions between the Bi_2 and the QL slabs are of a weak covalent nature.[10] Assessed by the bond-length–bond-strength concept, the structure of Bi_4Te_3 has the weakest bonding at the slab boundaries.[17] Bi_4Te_3, as another phase of the Bi–Te binary system, exhibits many similar properties with Bi_2Te_3, which is comprised of almost the same QL slabs,[18] such as a very close a-axis lattice constant (around 4.4 Å) and being assigned to the same space group $R\bar{3}m$ (D^5_{3d}).[14]

For Bi_4Te_3, according to the group theory classification and Raman selection rules, it is expected that there are nine Raman-active modes corresponding to the six different frequencies at the Brillouin zone center: $3(E_g + A_{1g})$.[13] The Raman tensors of the six Raman-active modes are as follow:

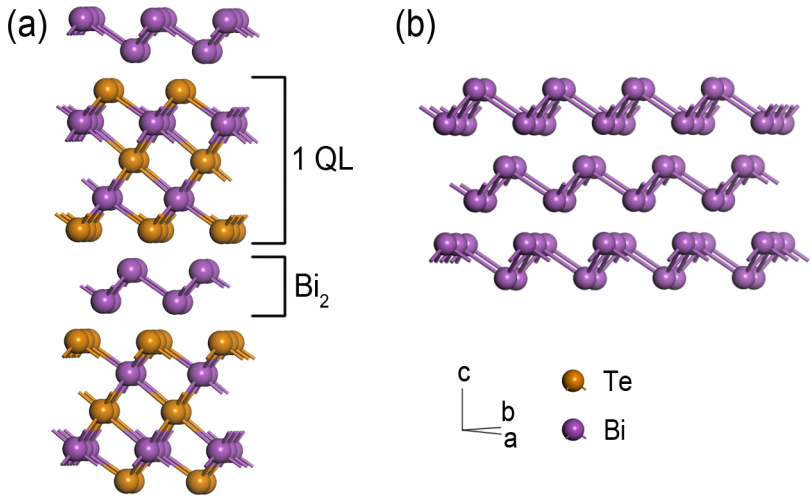

FIG. 1. Crystal structures of Bi_4Te_3 and Bi films with the same symmetry properties and similar lattice constants. The orange spheres denote tellurium atoms while the purple spheres denote bismuth atoms. (a) Crystal structure stacking along the c axis of Bi_4Te_3 films. (b) The layered structure of Bi films.

$$E_g = \begin{pmatrix} c & 0 & 0 \\ 0 & -c & d \\ 0 & d & 0 \end{pmatrix} \text{ or } \begin{pmatrix} 0 & -c & -d \\ -c & 0 & 0 \\ -d & 0 & 0 \end{pmatrix},$$

$$A_{1g} = \begin{pmatrix} a & 0 & 0 \\ 0 & a & 0 \\ 0 & 0 & b \end{pmatrix}.$$

Here, the letters "E" and "A" related to symmetry represent in-plane and out-plane (C_H axis) lattice vibrations, respectively. The subscript "g" standing for gerade denotes Raman-active. The six eigenpeaks can be assigned to E_g^1 (TO), E_g^2 (TO), E_g^3 (TO), A_{1g}^1 (LO), A_{1g}^2 (LO), A_{1g}^3 (LO) modes based on their wavenumbers and corresponding oscillation modes, respectively.

The arrangement of the Bi_2 atoms in Bi_4Te_3 films have particularly similar properties to those in bismuth films, for example, the symmetry properties, the length of Bi-Bi bond, a-axis lattice constant[19] and so forth. So the structural properties of the Bi_2 slabs in Bi_4Te_3 could refer to those in bismuth films, which crystallize in a rhombohedral A7 structure and belong to the space group D_{3d}^5, as well as Bi_2Te_3 and Bi_4Te_3.[20] Regarding bismuth films, they have a layered structure like Bi_4Te_3, consisting of stacks of Bi_2 atoms (see Fig. 1(b)). Based on the bonding abilities of Bi governed by its 6p orbitals,[15] each Bi atom is bonded to three intra-bilayer partners at 3.07 Å and to three inter-bilayer partners at 3.53 Å. As a result, each Bi atom has three nearest-neighbor bonds, forming the stable Bi_2 slabs with strong intra-bilayer covalent bonds in bismuth films.[15,21]

Bi_4Te_3 films can be considered to have a structure where the Bi_2 slab is inserted into the Bi_2Te_3 film structure periodically.[10,22] Taking into account the properties of the Bi_2 atoms, the Bi_2 slabs in Bi_4Te_3 can be further viewed as ultrathin Bi films with a thickness of only one bilayer. The equivalent model above suggests that Bi_4Te_3 is expected to exhibit some of the specific properties arising from both Bi and Bi_2Te_3 films.

B. Raman spectra analysis

Figure 2(a) shows the measured Raman spectra of a 50 nm Bi_4Te_3 film with changing intensity of the excitation laser power and exposure time (the obtained spectra from the other three 50 nm samples remain the same). The frequencies of the observed peaks almost remain the same with

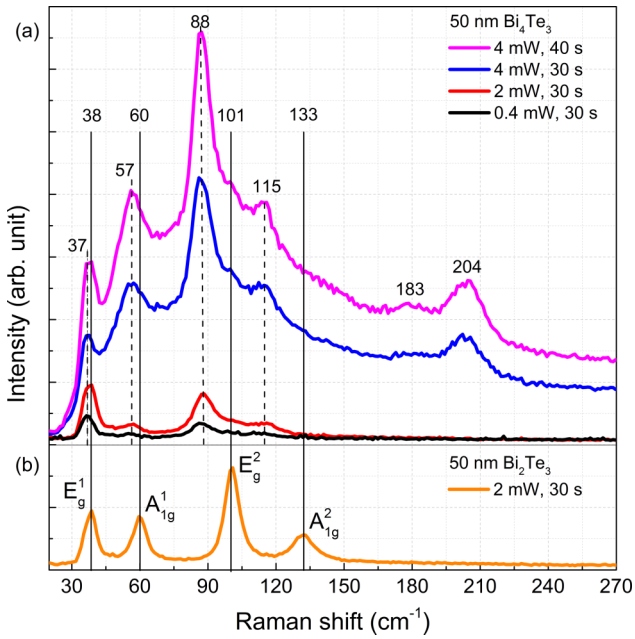

FIG. 2. Raman spectra of 50 nm thick Bi_2Te_3 and Bi_4Te_3 films grown on Si by MBE. (a) Raman spectra of a Bi_4Te_3 film with changing excitation power and exposure time. (b) Raman spectrum of a Bi_2Te_3 film with the four eigenpeaks labelled.

increasing excitation power and irradiation time, indicating that no laser-irradiation-induced damage occurred at these powers and irradiation times.[23] When the excitation power was increased to 4 mW, the intensity of the peaks in the spectra were all strengthened, together with the appearance of new peaks. Peaks at 88 and 115 cm^{-1} were both pronounced and assigned to the Raman eigenpeaks of Bi_4Te_3 films. The reason for these assignments is two-fold. First, the peak at 88 cm^{-1} has been reported and interpreted to arise from the vibrational mode of Bi_4Te_3 films in Ref. 13, although this peak was observed at 83 cm^{-1} in that study, probably owing to systemic errors (the peak positions of Bi_2Te_3 in Ref. 13 all experienced around a five wavenumber redshift compared with the standard values[24]). Second, Yang *et al.*[25] predicted theoretically that the phonon dispersions of ultrathin Bi films with only one bilayer thickness have frequencies for the E_g (TO) mode and A_{1g} (LO) mode of 92 cm^{-1} and 115.3 cm^{-1} (both are Raman-active), respectively, at the Brillouin zone center, which are listed in Table I. To our best knowledge, there has been no publication reporting the experimental Raman results of ultrathin Bi films whose thickness is down to the atomic layer level, although Ref. 13 reported two measured Raman peaks of Bi films at around 65 cm^{-1} and 91 cm^{-1}. It is worth noting that when the thickness of materials decreases from 3D to 2D, the Raman peak positions are expected to be shifted.[26] Taking the calculation and experimental errors into account, the theoretical results are consistent with the observed peaks at 88 and 115 cm^{-1} in Bi_4Te_3, indicating that both peaks can be credibly attributed to the vibrational modes of Bi_2 slabs in Bi_4Te_3 films and are therefore assigned to the E_g (TO) and A_{1g} (LO) modes, respectively.

TABLE I. Frequencies (cm^{-1}) of Raman peaks in Bi_4Te_3, Bi_2Te_3 and ultrathin Bi films.

	E_g^1 (TO)	A_{1g}^1 (LO)	E_g (TO)	E_g^2 (TO)	A_{1g} (LO)	A_{1g}^2 (LO)			
Bi film (one bilayer)[25]			92		115.3				
Bi_2Te_3 film (50 nm)	38.0	59.7		101.1		132.7			
Bi_2Te_3 film (50 nm)[24]	39	61.1		101.5		132.4			
	P1	**P2**	**P3**	**P4**	**P5**	**P6**	**A1**	**A2**	**A3**
Bi_4Te_3 film (50 nm)	37.2	57.1	87.7	100.0	114.9	132.2	74.2	182.8	204.2

Figure 2(b) shows the obtained Raman spectrum of a 50 nm Bi_2Te_3 film, in which the four eigenpeaks are highlighted by the black solid lines. The frequencies and assignments of these four peaks are listed in Table I and are comparable with the previously reported data.[24] It is particularly noticeable that the three eigenpeaks at lower frequencies of the Bi_2Te_3 film can also be directly observed in the spectra of Bi_4Te_3 films. In Figure 2(a), the E_g^1 and the A_{1g}^1 modes are distinct, albeit with a few wavenumber redshift, while the E_g^2 mode is obscured when the irradiation power was below 2 mW. When the irradiation power and exposure time was increased to 4 mW and 40 s, respectively, the E_g^2 mode can also be pronouncedly observed.

The A_{1g}^2 mode of Bi_2Te_3 films can be distinguished from the spectra of Bi_4Te_3 films by multiple peak fitting. Figure 3 displays the Raman spectrum of a Bi_4Te_3 film under 4 mW excitation (the blue curve in Fig. 2(a)), which is analyzed by Gaussian fitting to decompose the overlapped peaks. According to the fitting results, the spectrum consists of nine separate peaks, which are labelled as shown in Fig. 3, whose frequencies are listed in Table I. P1, P2 and P4 correspond to the three Raman-active peaks at lower frequencies of Bi_2Te_3 films, and P3 and P5 have been analyzed above. As can be seen, the frequency of P6 is very close to that of the A_{1g}^2 mode of Bi_2Te_3 films.

The four Raman peaks of Bi_2Te_3 films correspond to the Raman-active oscillation modes (E_g^1 (TO), A_{1g}^1 (LO), E_g^2 (TO), A_{1g}^2 (LO)) involving the QL slabs. Furthermore, the structure of Bi_4Te_3 contains similar QL slabs, thus, it is reasonable to observe the similar peaks in the spectra of Bi_4Te_3 and assign P1, P2, P4 and P6 to the Raman eigenpeaks of Bi_4Te_3 films. Interestingly, these four peaks all develop a few wavenumber redshift when compared with the corresponding modes in Bi_2Te_3 films. The redshift in the spectra of Bi_4Te_3 films could be caused by the changed bonding at the boundaries between the Bi_2 and the QL slabs but the exact details need to be further studied.

The frequencies of P1–P6 are assigned to the E_g^1 (TO), A_{1g}^1 (LO), E_g^2 (TO), E_g^3 (TO), A_{1g}^2 (LO), and A_{1g}^3 (LO) modes, respectively. To the best of our knowledge, all six of the Raman modes predicted by group theory have been observed and resolved entirely for the first time in the Raman spectra of Bi_4Te_3. The band-structure calculation suggests that Bi_4Te_3 can be easily exfoliated and terminated with an intact Bi_2 slab or QL slab.[8] Owing to the weak bonding at the slab boundaries, P1, P2, P4 and P6 are involved with QL slabs while P3 and P5 primarily arise from Bi_2 slabs. Therefore, Raman-active phonon oscillations in Bi_4Te_3 films exhibit the vibrational properties of those in both Bi and Bi_2Te_3 films.

In Fig. 3, in addition to the six expected peaks, there are three additional peaks (A1 to A3), and their frequencies are listed in Table I. It is worth noting that A1 was also observed in the Raman

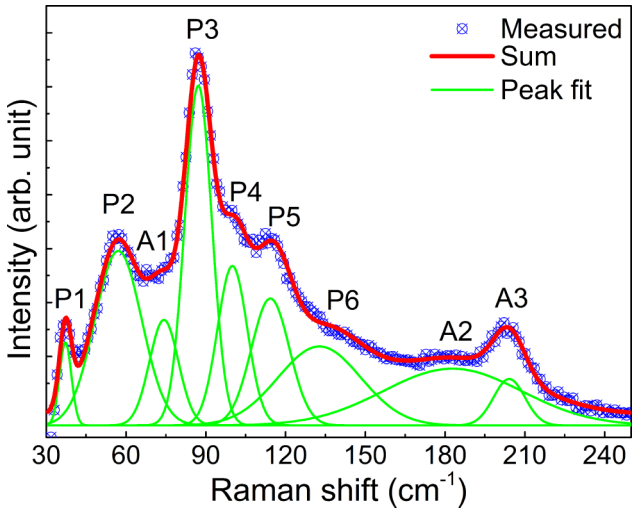

FIG. 3. Raman spectrum of a 50 nm Bi_4Te_3/Si thin film obtained under 4 mW irradiation power of 532 nm excitation laser (corresponding to the blue curve in Fig. 2(a)). The blue dotted curve is the measured spectrum, the green curves are the fitted peaks with a Gaussian line-shape, and the red curve is the sum of these fitted peaks.

spectra of the 20–50 nm Bi_2Te_3 films, where A1 has been ascribed to surface oxidation for the reason that Bi_2Te_3 films are easily oxidized on the surface when exposed in the air.[27] Similarly, A1 in the spectra of Bi_4Te_3 films is most likely to arise from the same origin. When the laser power was increased to 4 mW, A2 (182 cm^{-1}) and A3 (204 cm^{-1}) began to appear (see Fig. 2(a)) and the eigenpeak of Si substrate at 520.5 cm^{-1} began to be observed, indicating that A2 and A3 most possibly result from the LHE-induced oxidation, and the laser penetration depth is larger than the thickness of Bi_4Te_3 films when the laser power is 4 mW. Comparing the frequencies of A2 and A3 with those of bismuth oxide and tellurium oxide,[28–30] A2 and A3 are tentatively assigned to the vibrational modes from α-Bi_2O_3 (185 cm^{-1}) and $Bi_{12}SiO_{20}$ (205 cm^{-1}), respectively.

IV. CONCLUSIONS

A Raman spectroscopy study was carried out for 50 nm Bi_4Te_3 films on Si substrates grown by MBE. The directly observed and fitted peaks in the Raman spectra are all assigned to the corresponding phonon modes. The structural properties of Bi_4Te_3 are introduced and the Raman tensors are investigated based on group theory and Raman selection rules. No Raman spectra of Bi_4Te_3 films with the six complete expected peaks have been previously published. Based on the frequencies and assignments of the six eigenpeaks, Raman-active phonon oscillations in Bi_4Te_3 films are found to exhibit the vibrational properties of those in both Bi and Bi_2Te_3 films.

ACKNOWLEDGEMENTS

The authors would like to thank Kun Wang, from Shanghai Institute of Applied Physics, Chinese Academy of Sciences, for his help with Raman measurements and Jiqiang Ning, from The University of Hong Kong, for the fruitful discussions. The financial support from the Natural Science Foundation of China (Grant No. 61404153), the Shanghai Pujiang Program (Grant No.14PJ1410600), the Key Program of Natural Science Foundation of China (Grant No. 61334004), the National Basic Research Program of China (973) (Grant No. 2014CB643902), Strategic Priority Research Program of the Chinese Academy of Sciences (Grant No. XDA5-1), the Key Research Program of the Chinese Academy of Sciences (Grant No. KGZD-EW-804), the Creative Research Group Project of Natural Science Foundation of China (Grant No. 61321492) and the International Collaboration and Innovation Program on High Mobility Materials Engineering of Chinese Academy of Sciences is acknowledged.

[1] H. J. Zhang, C. X. Liu, X. L. Qi, X. Dai, Z. Fang, and S. C. Zhang, Nat. Phys. **5**, 438 (2009).
[2] Y. L. Chen, J. G. Analytis, J. H. Chu, Z. K. Liu, S. K. Mo, X. L. Qi, H. J. Zhang, D. H. Lu, X. Dai, Z. Fang, S. C. Zhang, I. R. Fisher, Z. Hussain, and Z. X. Shen, Science **325**, 178 (2009).
[3] M. Z. Hasan and C. L. Kane, Rev. Mod. Phys. **82**, 3045 (2010).
[4] J. E. Moore, Nature **464**, 194 (2010).
[5] F. J. DiSalvo, Science **285**, 703 (1999).
[6] M. S. Dresselhaus, G. Dresselhaus, X. Sun, Z. Zhang, S. B. Cronin, and T. Koga, Phys. Solid State **41**, 679 (1999).
[7] R. Venkatasubramanian, E. Siivola, T. Colpitts, and B. O'Quinn, Nature **413**, 597 (2001).
[8] Hanna Lind, Sven Lidin, and Ulrich Häussermann, Phys. Rev. B **72**, 184101 (2005).
[9] H. Lind and S. Lidin, Solid State Sci. **5**, 47 (2003).
[10] J. W. G. Bos, H. W. Zandbergen, M. H. Lee, P. Ong, and R. J. Cava, Phys. Rev. B **75**, 195203 (2007).
[11] T. Hirahara, G. Bihlmayer, Y. Sakamoto, M. Yamada, H. Miyazaki, S. Kimura, S. Blugel, and S. Hasegawa, Phys. Rev. Lett. **107**, 166801 (2011).
[12] A. Fulop, Y. X. Song, S. Charpentier, P. X. Shi, M. Ekstrom, L. Galletti, R. Arpaia, T. Bauch, F. Lombardi, and S. M. Wang, Appl. Phys. Express **7**, 045503 (2014).
[13] V. Russo, A. Bailini, M. Zamboni, M. Passoni, C. Conti, C. S. Casari, A. L. Bassi, and C. E. Bottani, J. Raman Spectrosc. **39**, 205 (2008).
[14] K. Yamana, K. Kihara, and T. Matsumoto, Acta Crystallogr., Sect. B: Struct. Sci. **35**, 147 (1979).
[15] A. Isaeva, B. Rasche, and M. Ruck, Phys. Status Solidi RRL **7**, 39 (2013).
[16] W. Richter and C. R. Becker, Phys. Status Solidi B **84**, 619 (1977).
[17] N. E. Brese and M. Okeeffe, Acta Crystallogr., Sect. B: Struct. Sci. **47**, 192 (1991).
[18] J. O. Jenkins, R. W. Ure, and J. A. Rayne, Phys. Rev. B **5**, 3171 (1972).
[19] V. Chis, G. Benedek, P. M. Echenique, and E. V. Chulkov, Phys. Rev. B **87**, 075412 (2013).
[20] H. Monig, J. Sun, Y. M. Koroteev, G. Bihlmayer, J. Wells, E. V. Chulkov, K. Pohl, and P. Hofmann, Phys. Rev. B **72**, 085410 (2005).

[21] Y. M. Koroteev, G. Bihlmayer, E. V. Chulkov, and S. Bluegel, Phys. Rev. B **77**, 045428 (2008).
[22] Y. Kim, S. L. Cho, A. DiVenere, G. K. L. Wong, and J. B. Ketterson, Phys. Rev. B **63**, 155306 (2001).
[23] D. Teweldebrhan, V. Goyal, and A. A. Balandin, Nano Lett. **10**, 1209 (2010).
[24] K. M. F. Shahil, M. Z. Hossain, V. Goyal, and A. A. Balandin, J. Appl. Phys. **111**, 054305 (2012).
[25] J. Yang, G. Q. Huang, and X. F. Zhu, Phys. Status Solidi B **250**, 1937 (2013).
[26] J. Zhang, Z. Peng, A. Soni, Y. Zhao, Y. Xiong, B. Peng, J. Wang, M. S. Dresselhaus, and Q. Xiong, Nano Lett. **11**, 2407 (2011).
[27] H. Xu, Y. X. Song, Q. Gong, W. W. Pan, X. Y. Wu, and S. M. Wang, Mod. Phys. Lett. B **29**, 1550075 (2015).
[28] AJ Salazar-Pérez, MA Camacho-López, RA Morales-Luckie, V Sánchez-Mendieta, F Ureña-Núñez, and J Arenas-Alatorre, Superficies y vacío **18**, 4 (2005).
[29] A. S. Pine and G. Dresselhaus, Phys. Lett. B **5**, 4087 (1972).
[30] J. Guo, F. Qiu, Y. Zhang, H. Deng, G. Hu, X. Li, G. Yu, and N. Dai, Chin. Phys. Lett. **30**, 106801 (2013).